Electronic Supplementary Material (ESI) for ChemComm.

Supporting Information

Near-unity angular anisotropy of circularly polarized luminescence from microspheres of monodispersed chiral conjugated polymer

Sota Nakayama,[1] Hiroshi Yamagishi, [1] * Osamu Oki, [1] Soh Kushida, [1] Junhui Chen, [1] Junpei Kuwabara, [1] Takaki Kanbara, [1] Wijak Yospanya, [2] Reiko Oda [3,2] and Yohei Yamamoto [1] *

[1] Department of Materials Science, Institute of Pure and Applied Sciences, and Tsukuba Research Center for Energy Materials Science (TREMS), University of Tsukuba, 1-1-1 Tennodai, Tsukuba, Ibaraki 305-8573, Japan

[2] Advanced Institute of Material Research (AIMR), Tohoku University 2-1-1 Katahira, Aoba, Sendai, Miyagi, 980-8577, Japan.

[3] University of Bordeaux, CNRS, Bordeaux INP, CBMN, UMR 5248, F-33600 Pessac, France

*e-mail: yamagishi.hiroshi.ff@u.tsukuba.ac.jp
yamamoto@ims.tsukuba.ac.jp

1. General

Materials and Methods.
All reagents and solvents were purchased from Sigma–Aldrich, TCI, Acros Organics and Merck. The compound 2,2′-(9,9- bis((*S*)-3,7-dimethyloctyl)-9*H*-fluorene-2,7-diyl)bis(4,4,5,5,-tetramethyl-1,3,2- dioxaborolane) (1) and 4,7-dibromobenzothiadiazole (2) were purchased from 1-Material Inc. and Sigma–Aldrich. Unless otherwise noted, all reagents and solvents were used as received. Chiral copolymer, Poly(9,9'-bis((*S*)-3,7-dimethyloctyl)-2,7-fluorene-*alt* benzothiadiazole), ((*S*,*S*)-PFBT), (Fig. 2a) was synthesized according to the reported procedure similar to that employed for the synthesis of ((*R*,*R*)-PFBT)[S1]. Photoabsorption spectra were measured on a JASCO V-630 spectrophotometer using quartz cuvette with a pathlength of 1 mm. Steady-state PL spectra were recorded on a JASCO FP-8300 spectrofluorometer. Scanning electron microscopy (SEM) was performed on a Hitachi Model S-3700N SEM operating at 20 kV. Optical microscopy (OM), fluorescence microscopy (FM) and polarized optical microscopy (POM) observations were carried out using an Olympus model BX53 upright microscope. Differential scanning calorimetry (DSC) analysis was conducted on a Seiko Instruments Inc. model EXSTAR7000: X-DSC7000 in a temperature range from –10 to 135°C at a heating rate of 5°C min^{-1} under constant Ar flow. NMR spectra were recorded on a JEOL JEM-ECS-400 NMR spectrometer operated at 400 MHz for ^{1}H and 100 MHz for ^{13}C nuclei. Chemical shifts are reported in ppm and calibrated against residual solvent peaks (7.26 ppm for ^{1}H and 77.16 ppm for ^{13}C). Peak multiplicity are abbreviated as; singlet (s), doublet (d), triplet (t) and multiplet (m). Size exclusion chromatography (SEC) was performed on Japan Analytical Industry model LC-9210 II NEXT equipped with a GPC column (JAIGEL-2HH). Samples were prepared in $CHCl_3$, and the solution were filtered through a 0.2 μm PTFE filter before measurement. The polymer was fractionated based on the molecular weight by using this apparatus, and we set the interval for collecting the fractions as 20 s on average to make their PDI as narrow as possible. The photoluminescence quantum yields were measured using Hamamatsu model C9920-02 absolute PL quantum yield measurement system.

Preparation of Microspheres
For vapor diffusion method, a 2 mL vial containing a $CHCl_3$ solution of (*S,S*)-PFBT (0.5 mg mL^{-1}, 500 μL) was placed in a 20 mL vial with 2.5 mL of MeOH as a poor solvent. The out-side vial was capped and then allowed to stand for 1 day at 25°C. The MeOH vapor was slowly diffused into the solution, resulting a precipitation of the polymeric microspheres of (*S*,*S*)-PFBT after the supersaturated state (Fig. 1a). The microspheres were cast onto a glass plate, and their size, morphology, and locations were observed with the optical microscope. In the meantime, a microsphere with an optimum diameter (4.0–4.5 μm) was picked up using a sharp tungsten needle that was controlled numerically by the micromanipulator (MicroSupport Model, Quick Pro) for the following CPL measurements.

CPL measurements
CPL measurements of suspensions of polymer microspheres were carried out by JASCO CPL-300 (λ_{ex} = 365 nm). CPL measurements of a single microsphere were carried out with our home-made microscopy setup (Fig. S22) according to our previous report[S1].

Depolarized cw laser (λ_{ex} = 405 nm, THOLABS model DPP25-A) was aligned into an objective lens (50X, NA = 0.42) and excited a single microsphere. Left- and right-handed CPL components were collected by using achromatic quarter wave plate (QWP, 465−610 nm) and polarizer in straight optical pass. Transmitted PL was collected by an objective and detected by a spectrometer (Ocean Optics model FLAME-S-XR1-ES spectrometer, grating 500 grooves mm^{-1}) through an optical fibre with the spectral resolution of 0.46 nm.

The angle-average g_{lum} value $g_{lum}^{avg.}$ is defined as follows:

$$|g_{lum}^{avg.}| = \frac{|g_{lum}^{total}|}{S}$$
$$= \frac{8\int_0^{\frac{\pi}{2}}\int_0^{\frac{\pi}{2}}(a+b|\sin\theta|)r^2\sin\theta d\theta d\phi}{4\pi r^2}$$
$$= \frac{8r^2[-a\cos\theta+\frac{b\pi}{2}+\frac{b\sin 2\theta}{4}]_0^{\frac{\pi}{2}}[\phi]_0^{\frac{\pi}{2}}}{4\pi r^2}$$
$$= a+\frac{b}{4}\pi \qquad \text{eq. S1}$$

2. Synthesis

Synthesis of Poly(9,9'-bis((*S*)-3,7-dimethyloctyl)-2,7-fluorene-*alt*-benzothiadiazole) ((*S*,*S*)-PFBT). The synthesis route of (*S*,*S*)-PFBT was established according to our previous report [S1]. To focus on the oligomers, the amount of solvent (1,4-dioxane: water (2:1)) was reduced to 18 mL in the synthesis.

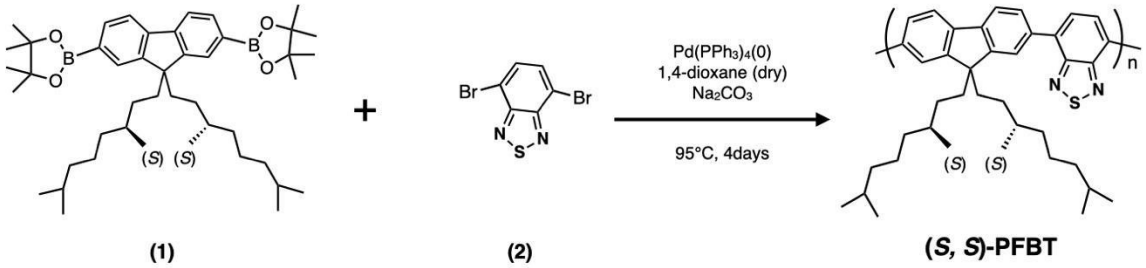

Scheme.S1. Synthetic route of (*S*,*S*)-PFBT

Synthesis of (*S*,*S*)-PFBT : 2,2′-(9,9-bis((*S*)-3,7-dimethyloctyl)-9*H*-fluorene-2,7-diyl)bis(4,4,5,5,-tetramethyl-1,3,2- dioxaborolane) (1) (500 mg, 0.71 mmol, 1.0 eq.), 4,7-dibromobenzothiadiazole (2) (210 mg, 0.71 mmol, 1.0 eq.), and sodium carbonate (793 mg, 7.48 mmol, 10.5 eq.) were charged into 50 mL Schlenk flask fitted with a N_2 inlet. The contents of the Schlenk flask were evacuated and filled with N_2 gas for three times. tetrakis(triphenylphosphine)-palladium(0) (69 mg, 0.060 mmol, 0.08 eq.) and a degassed mixture of 1,4-dioxane:water (2/1 *v*/*v*, 18 mL) by N_2 gas bubbling were added under N_2 gas counterflow. The contents of the flask were heated to 95°C for 4 days under dark and closed system. The reaction mixture was allowed to cool down to the room temperature,

and dark yellow precipitation was obtained.

Purification: The contents were transferred to another flask by chloroform solution. Sodium *N*, *N*-diethyldithiocarbamate aqueous solution (10 g L^{-1}, 100 mL) was added to chelate the residual palladium catalyst and the solution was stirred at room temperature for 1 day. The contents were transferred again to a separating funnel using chloroform, and the organic layer was collected. After that, the organic layer was sequentially washed with 1M HCl (2 × 100 mL), 28% aqueous ammonia solution (2 × 100 mL), and finally with brine (1 × 100 mL). The solution was dried over anhydrous sodium sulphate and evaporated until few mL of the solvent was left. The organic layer was concentrated and added to methanol (250 mL) in a dropwise manner The yellowish-orange solid was washed with excess methanol and collected by filtration and drying in vacuo at 60°C for 6 h. (270 mg, 65% yield).

Fractionation: The crude was dissolved in chloroform, and subsequently subjected to preparative size exclusion chromatography. The solvent was separately evaporated, and the polymer fractions were obtained after reprecipitation into methanol, filtration, and drying in vacuo.

^{1}H-NMR (400 MHz, $CDCl_3$) : δ = 8.17–8.05 (m), 8.05–7.87 (m), 7.83–7.37 (m), 2.14 (m), 1.47–1.30 (m), 1.30–0.84 (m), 0.84–0.64 (m) ppm.

GPC (PS standard, $CHCl_3$): apparent M_n: 2.39 kg mol^{-1}, M_w: 4.46 kg mol^{-1}, PDI (M_w/M_n) = 1.91.

3. Supporting Figures.

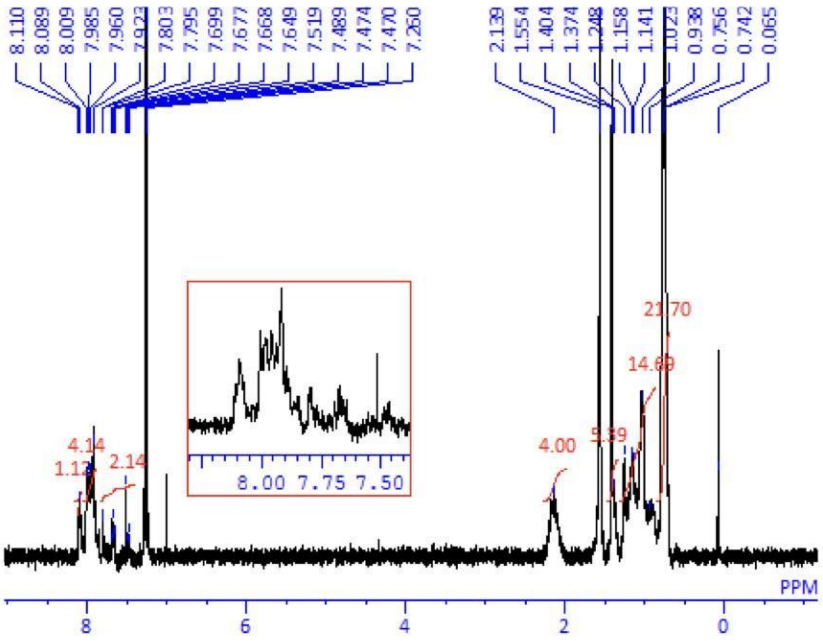

Fig. S1. ^{1}H-NMR (400 MHz, $CDCl_3$) spectrum of (*S*,*S*)-PFBT.

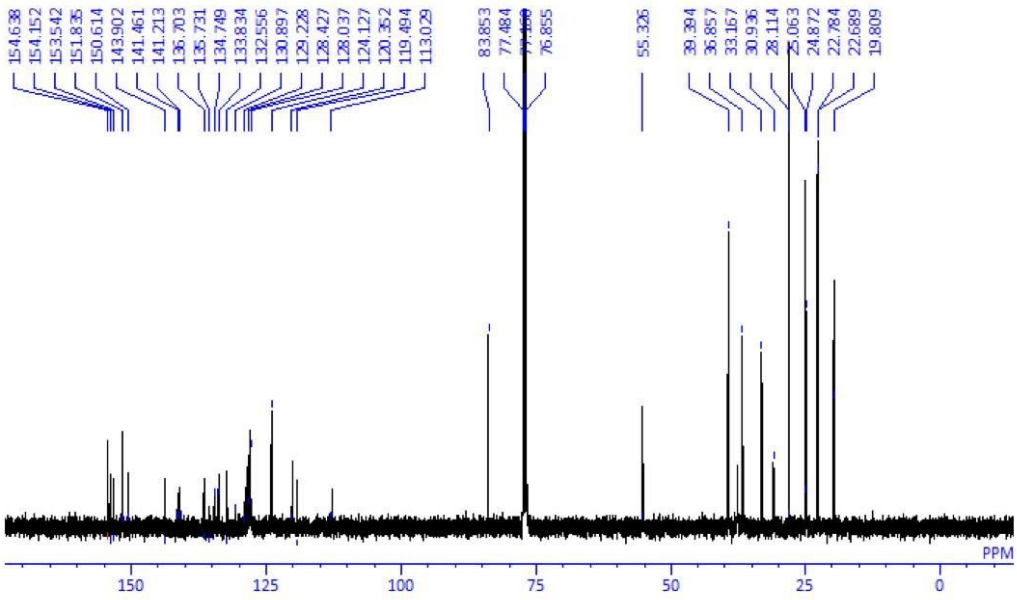

Fig. S2. ^{13}C-NMR (100 MHz, $CDCl_3$) spectrum of (*S*,*S*)-PFBT.

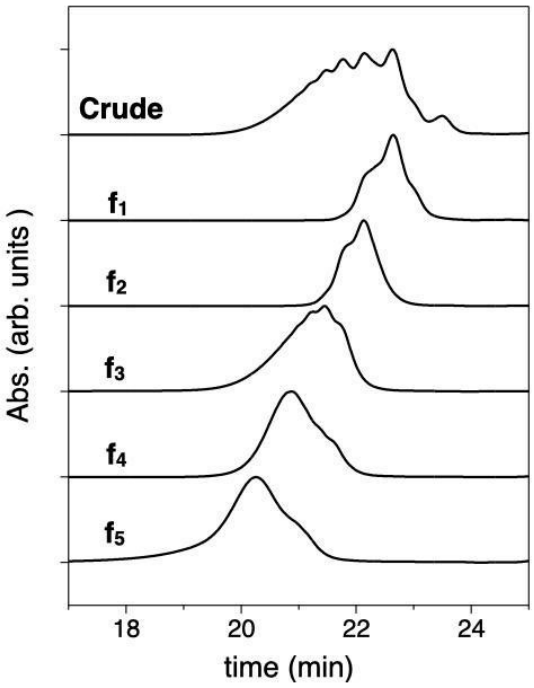

Fig. S3. Analytical SEC traces of (*S*,*S*)-PFBT crude and after fractionation.

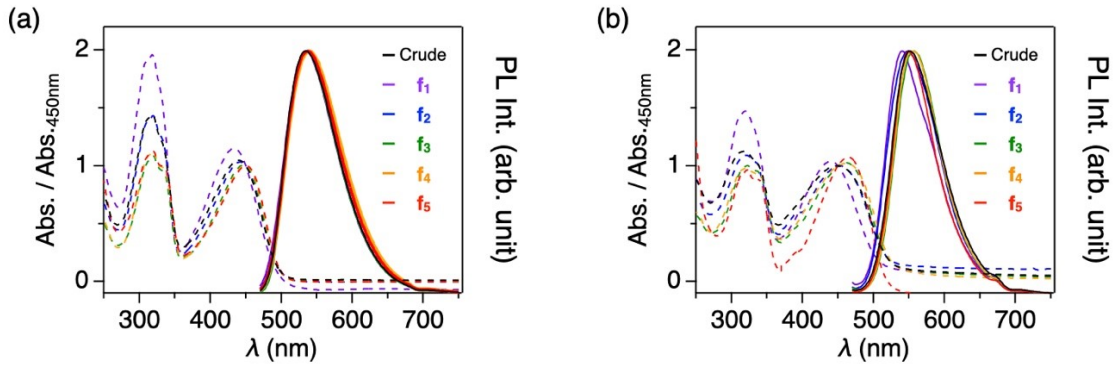

Fig. S4. UV-vis absorption (dashed lines) and emission (solid lines, λ_{ex} = 450 nm) spectra of (*S*,*S*)-PFBT crude and after fractionation in (a) $CHCl_3$ solution and in (b) cast film.

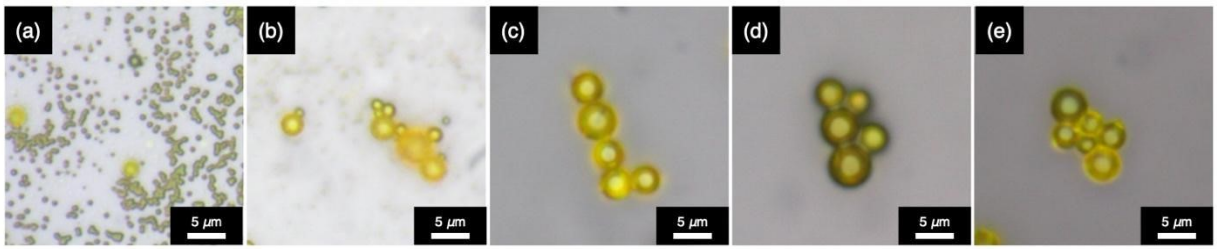

Fig. S5. Optical micrographs of self-assembled microstructures of (a) $\mathbf{f_1}$, (b) $\mathbf{f_2}$, (c) $\mathbf{f_3}$, (d) $\mathbf{f_4}$, (e) $\mathbf{f_5}$, respectively.

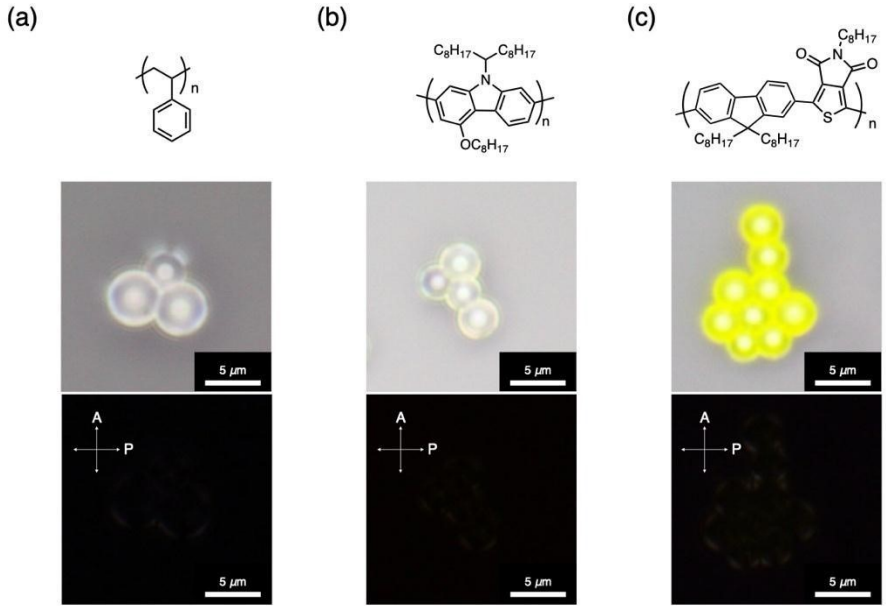

Fig. S6. Molecular structures, optical and POM micrographs of self-assembled (a) polystyrene[S2], (b) poly(9-(heptadecan-9-yl)-4-(octyloxy)-9*H*-carbazole)[S3] and (c) poly((9,9-dioctylfluorene-2,7-diyl)-*alt*-(5-octylthieno[3,4-c]pyrrole-4,6-dione-1,3-diyl)[S4] microspheres prepared by vapor diffusion method, respectively.

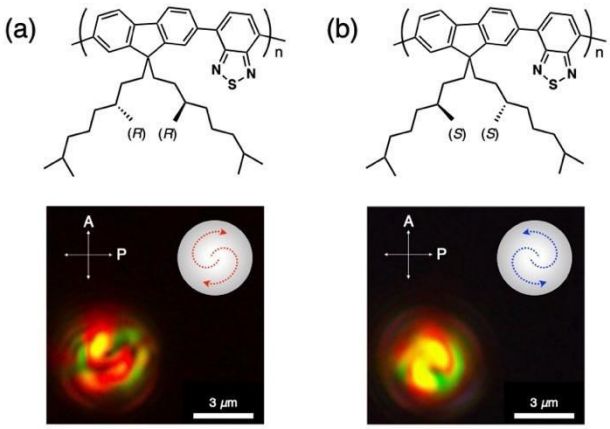

Fig. S7. Molecular structures and POM micrographs of self-assembled (a) (*R*,*R*)-PFBT and (b) (*S*,*S*)-PFBT microspheres [S1].

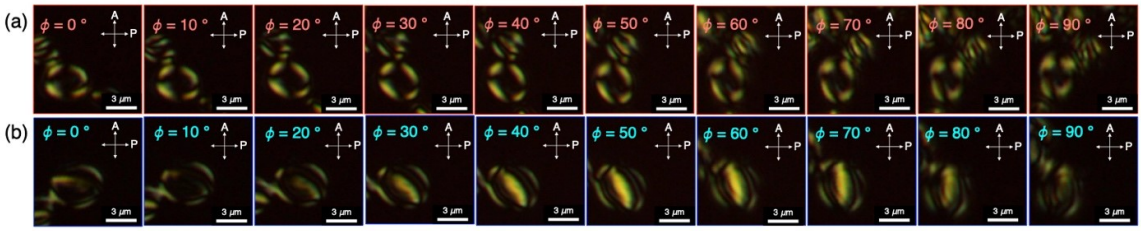

Fig. S8. POM micrographs of a sliced (*S*,*S*)-**MS$_{f3}$** which shows (a) a circular stripe with a Maltese Cross and (b) an ellipsoidal stripe upon the in-plane rotation of the specimens.

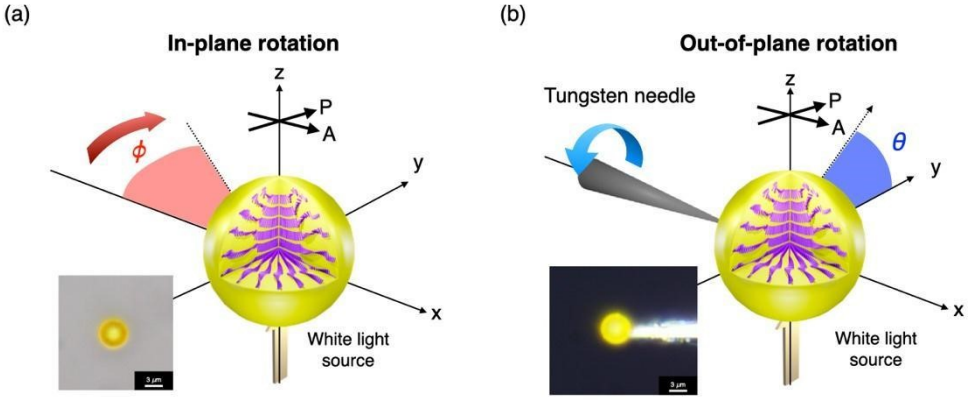

Fig. S9. Schematic representations of angle-dependent POM analysis of (*S*,*S*)-**MS** for (a) in-plane (ϕ) rotation and (b) out-of-plane (θ) rotation. Inset micrographs show the optical microscope images of a single (*S*,*S*)-**MS$_{f3}$** (a) on a thin glass substate and (b) picked up by a sharp tungsten needle.

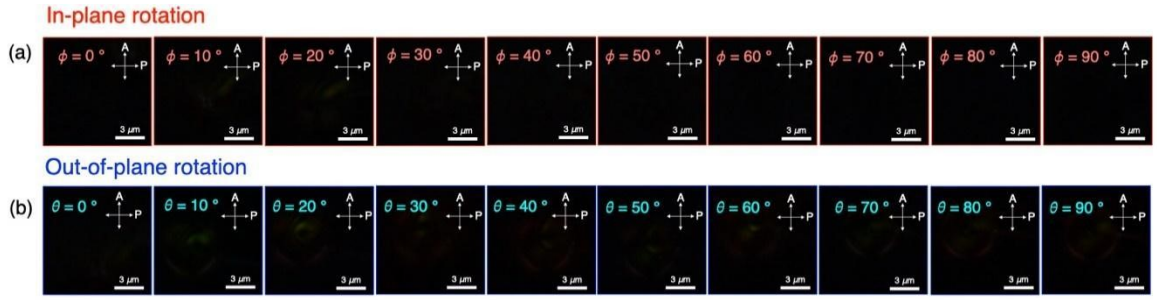

Fig. S10. Angle-dependent POM micrographs (*S,S*)-$\mathbf{MS_{f1}}$ for (a) in-plane (ϕ) rotation and (b) out-of-plane (θ) rotation.

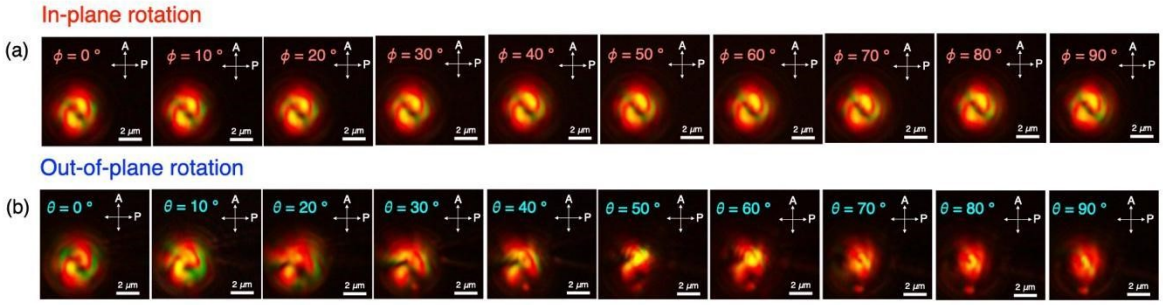

Fig. S11. Angle-dependent POM micrographs (*S,S*)-$\mathbf{MS_{f2}}$ for (a) in-plane (ϕ) rotation and (b) out-of-plane (θ) rotation.

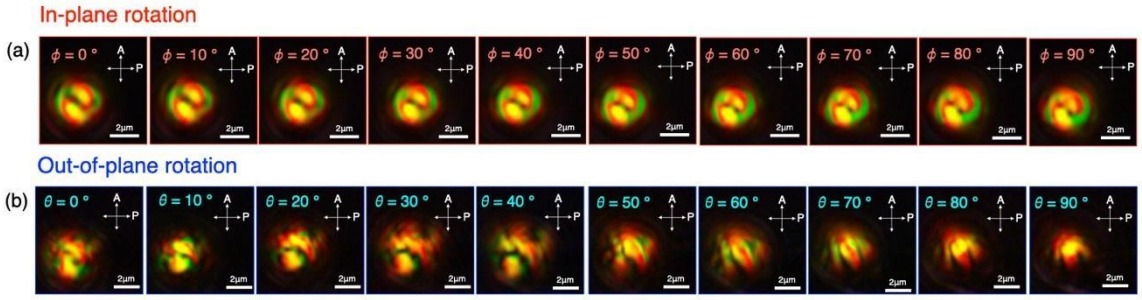

Fig. S12. Angle-dependent POM micrographs (*S,S*)-$\mathbf{MS_{f3}}$ for (a) in-plane (ϕ) rotation and (b) out-of-plane (θ) rotation.

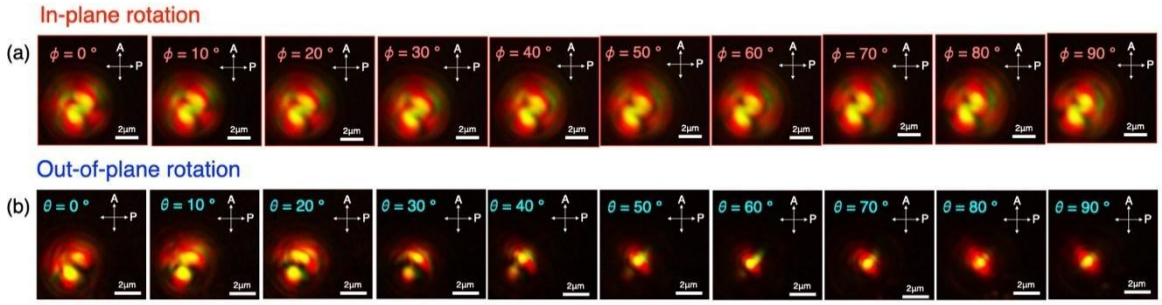

Fig. S13. Angle-dependent POM micrographs (*S,S*)-$\mathbf{MS_{f4}}$ for (a) in-plane (ϕ) rotation and (b) out-of-plane (θ) rotation.

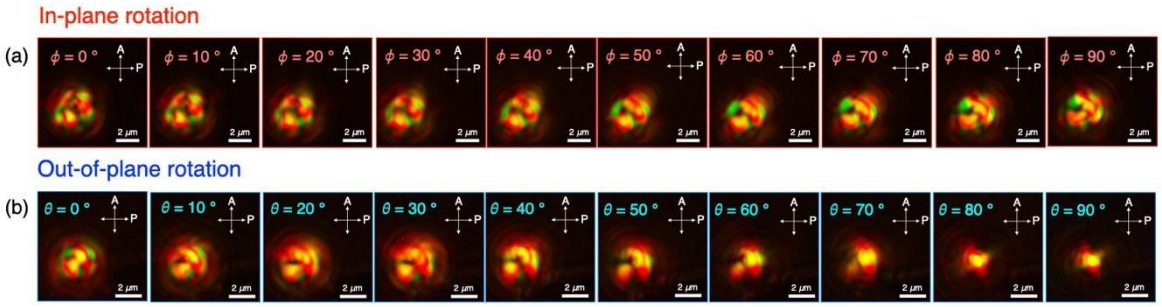

Fig. S14. Angle-dependent POM micrographs (*S,S*)-$\mathbf{MS_{f5}}$ for (a) in-plane (ϕ) rotation and (c) out-of-plane (θ) rotation.

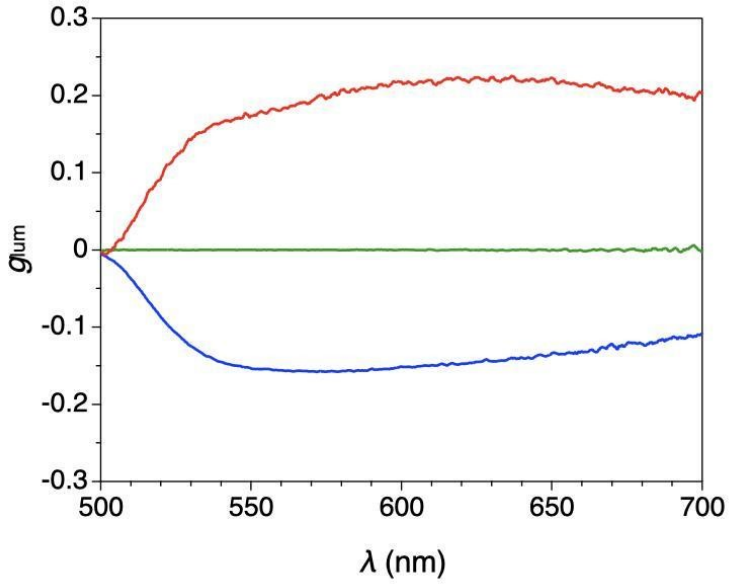

Fig. S15. CPL spectra (λ_{ex} = 365 nm) of MeOH suspension of (*S,S*)-**MS** (blue solid curve, $\mathbf{f_5}$), (*R,R*)-**MS** (red solid curve) and a-**MS** (green solid curve). A 2 mL aliquot of MeOH dispersion was measured for each **MS**. The dispersion was stirred during the measurements.

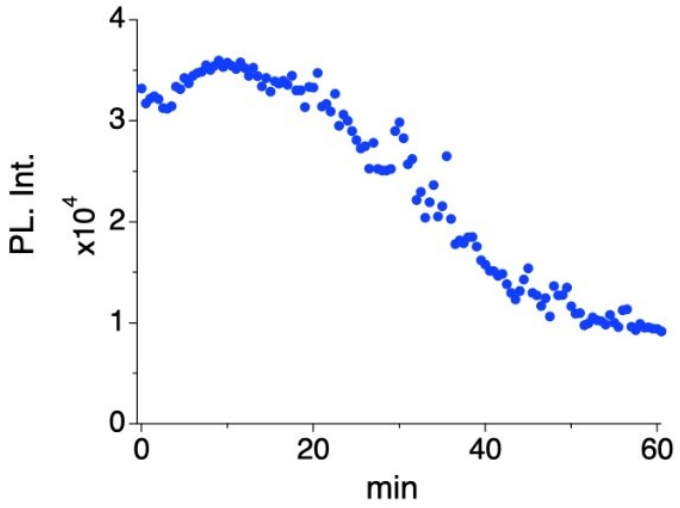

Fig. S16. Time-course change in photoluminescence intensity emitted from single $\mathbf{MS_{f2}}$ upon continuous photoexcitation (λ = 405 nm).

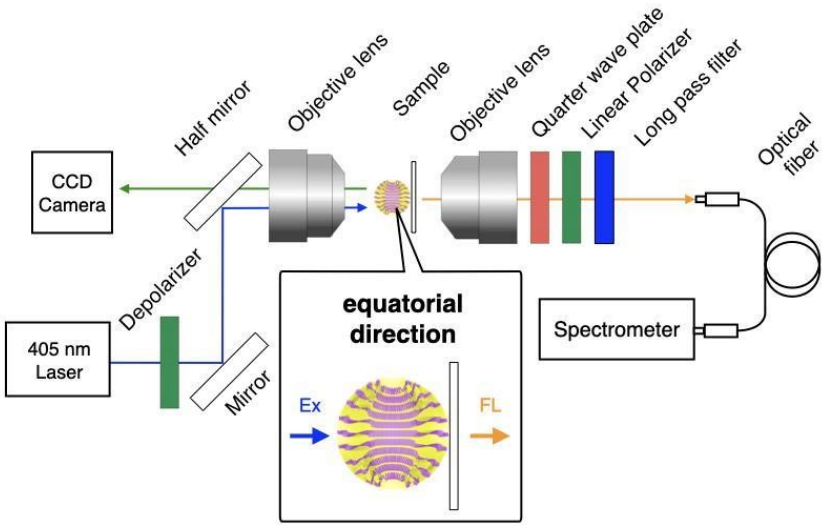

Fig. S17. Schematic representation of the experimental setup of CPL measurement from a single microsphere for equatorial direction (θ = 90°, 270°). A single microsphere was excited by a depolarized cw laser (λ_{ex} = 405 nm). PL from a single microsphere passes through an achromatic quarter wave plate (465−610 nm), a polarizer (400−700 nm), and a long-pass filter (working range: > 450 nm) in a straight-line pass.

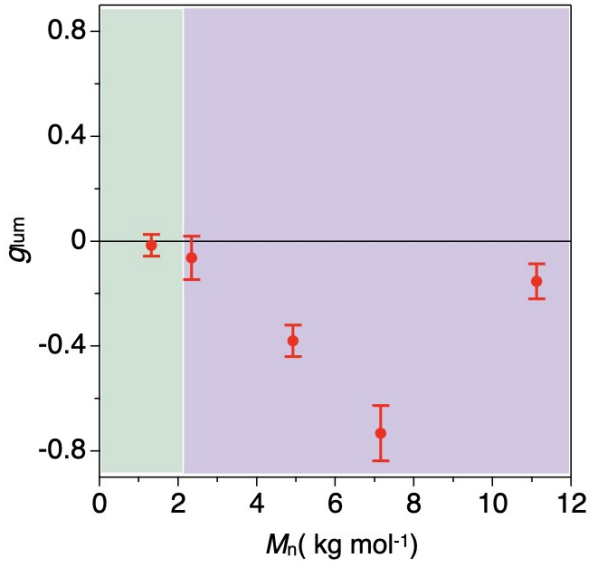

Fig. S18. Molecular wight dependence of $|g_{lum}|$ of CPL from a single (*S,S*)-**MS** along the equatorial direction (θ = 90°, 270°). Tens of (*S,S*)-**MS** with the diameter of 4.0−4.5 μm were picked up for all fractions.

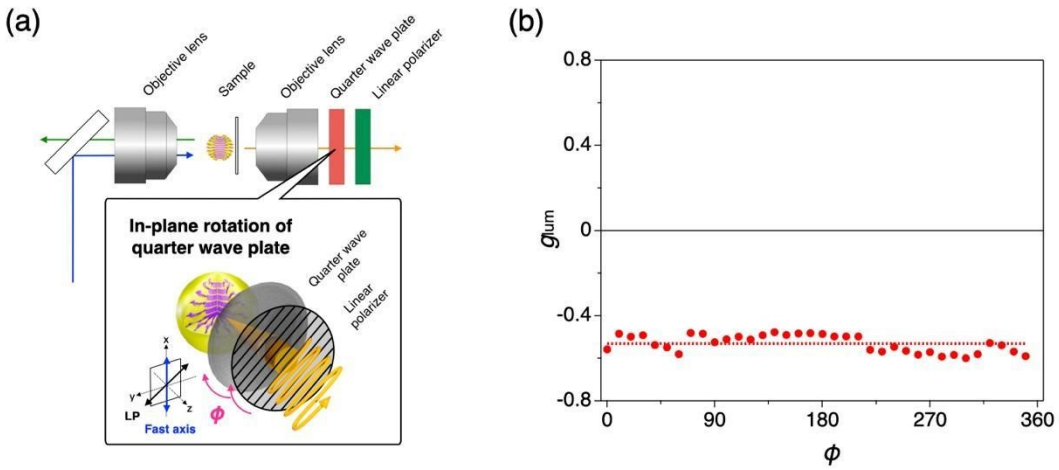

Fig. S19. (a) Schematic representation of angle dependent CPL measurement for (*S,S*)-**MS**$_{f3}$ against the in-plane rotational angle (ϕ) of the fast axis of QWP. (b) Plots of g_{lum} (at 546 nm) versus ϕ.

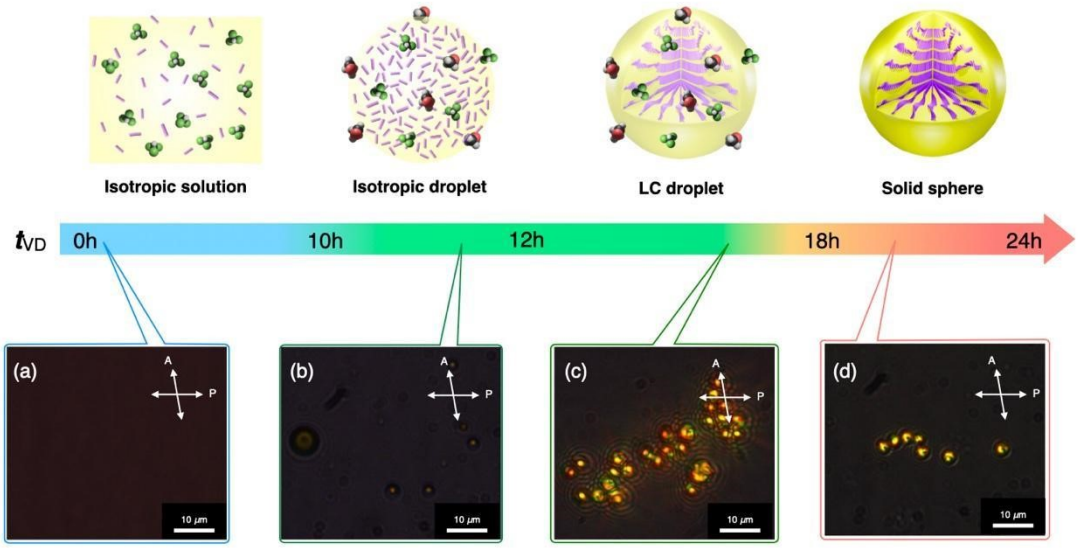

Fig. S20. Schematic representations of the formation process of (*S,S*)-**MS** with twisted bipolar molecular alignment. (a-d) Polarized optical micrographs of suspension of (*S,S*)-**MS**$_{f3}$ in $CHCl_3$/MeOH cosolvent from an (a) isotropic solution (t_{VD} = 0h), (b) isotropic droplet (t_{VD} = 11h), (c) LC droplet (t_{VD} = 17.5h) and (d) Solid microsphere (t_{VD} = 19.5h).

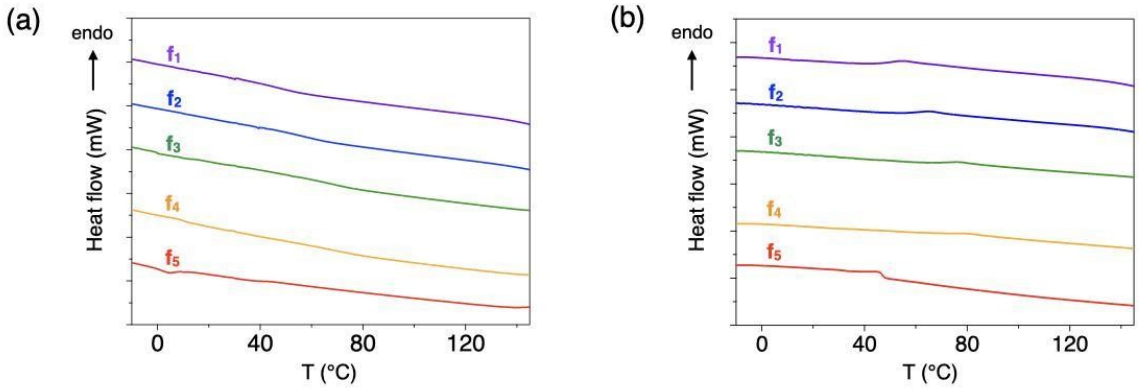

Fig. S21. DSC traces of (*S*,*S*)-PFBT fractions in (a) first cooling run and in (b) second heating run. Glass transition temperature (T_g) was 46.1 (**f**$_1$), 55.9 (**f**$_2$), 61.6 (**f**$_3$) and 70.1°C (**f**$_4$) calculated from the second heating run.

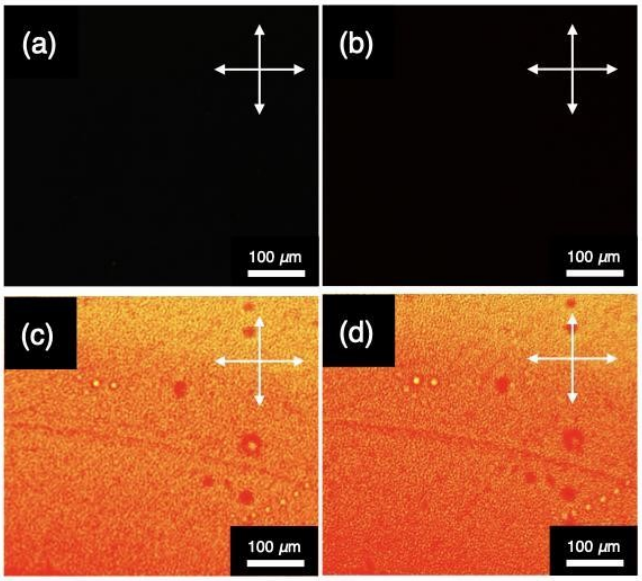

Fig. S22. POM micrographs of (a, b) **f**$_1$ and (c, d) **f**$_3$ cast films after (a, c) being heated at 135°C and (b, d) cooled down to 25°C.

Table S1. The parameters of sine fitting curve ($|g_{lum}|$ = a + b$|\sin\theta|$), the values of theoretical ($r_{theo.}$) and experimental ($r_{exp.}$) angular anisotropy in altitudinal coordinates of $|g_{lum}|$ at 546 nm from single (*S,S*)-**MS** in Fig. 4b, c.

	a	b	$r_{Theo.}$	$r_{Expt.}$
MS_{f1}	0	0	–	–
MS_{f2}	0.005	0.225	0.957	0.970
MS_{f3}	0.080	0.440	0.733	0.874
MS_{f4}	0.250	0.450	0.474	0.528
MS_{f5}	0.200	0.370	0.481	0.490

Table S2. Photoluminescence quantum yields when excited at 405 nm (ϕ_{PL}), $|g_{lum}^{avg.}|$, and the products of ϕ_{PL} and $|g_{lum}^{avg.}|$ of **MS**s.

	ϕ_{PL}	$\lvert g_{lum}^{avg.}\rvert$	$\phi_{PL} \times \lvert g_{lum}^{avg.}\rvert$
MS_{f1}	0.025	0	0
MS_{f2}	0.033	0.182	0.006
MS_{f3}	0.070	0.426	0.030
MS_{f4}	0.087	0.603	0.052
MS_{f5}	0.193	0.491	0.095

4. Supporting references

[S1] O. Oki, C. Kulkarni, H. Yamagishi, S. C. J. Meskers, Z. Lin, J. Huang, E. W. Meijer, and Y. Yamamoto, *J. Am. Chem. Soc.* 2021, **143**, 8772.

[S2] D. Okada, T. Nakamura, D. Braam, T. D. Dao, S. Ishii, T. Nagao, A. Lorke, T. Nabeshima and Y. Yamamoto, *ACS Nano* 2016, **10**, 7058.

[S3] S. Kushida, S. Okabe, T. D. Dao, S. Ishii, T. Nagao, A. Saeki, M. Kijima and Y. Yamamoto, *RSC Adv.*, 2016, **6**, 52854

[S4] S. Kushida, D. Braam, T. D. Dao, H. Saito, K. Shibasaki, S. Ishii, T. Nagao, A. Saeki, J. Kuwabara, T. Kanbara, M. Kijima, A. Lorke and Y. Yamamoto, *ACS Nano* 2016, **10**, 5543.